applied sciences

MDPI

Article

Heterogeneously Integrated Multicore Fibers for Smart Oilfield Applications

Xutao Wang [1], Honglin Sun [1], Huihui Wang [1], Zhiqun Yang [1,*], Yaping Liu [1,*], Zhanhua Huang [1] and Lin Zhang [1,2,*]

[1] Key Laboratory of Opto-Electronic Information Technology of Ministry of Education and Tianjin Key Laboratory of Integrated Opto-Electronics Technologies and Devices, School of Precision Instruments and Opto-Electronics Engineering, Tianjin University, Tianjin 300072, China
[2] Peng Cheng Laboratory, Shenzhen 518038, China
* Correspondence: yangzhiqun@tju.edu.cn (Z.Y.); liuyp@tju.edu.cn (Y.L.); lin_zhang@tju.edu.cn (L.Z.)

Abstract: In the context of Industry 4.0, the smart oilfield is introduced, which relies on large-scale information exchange among various parts, and there is an urgent need for special fiber links for both increased data transmission capacity and high-sensitivity distributed sensing. Multicore fibers can be expected to play a critical role, in the parts of cores that are responsible for data transmission, while others are used for sensing. In this paper, we propose a heterogeneously integrated seven-core fiber for interconnection and awareness applications in smart oilfields, which could not only support digital and analog signal transmission but could also measure temperature and vibration. The core for digital signal transmission has a low differential mode group delay of 10 ps/km over the C-band, and the crosstalk between adjacent cores is lower than −55 dB/km at the pitch of 50 μm. A 25-Gbaud transmission over 50 km is simulated. Each core for analog signal transmission has a large effective area of 172 μm^2 to suppress the nonlinear effect due to the watt-scale input power. The proposed heterogeneously multicore fiber exhibits great potential to be applied in smart oilfields, meeting the demand for efficient and cost-effective oil production.

Keywords: space division multiplexing; multicore fiber; Industry 4.0; smart oilfield

Citation: Wang, X.; Sun, H.; Wang, H.; Yang, Z.; Liu, Y.; Huang, Z.; Zhang, L. Heterogeneously Integrated Multicore Fibers for Smart Oilfield Applications. *Appl. Sci.* **2023**, *13*, 1579. https://doi.org/10.3390/app13031579

Academic Editor: Nuno Alexandre Peixoto Silva

Received: 21 December 2022
Revised: 18 January 2023
Accepted: 24 January 2023
Published: 26 January 2023

1. Introduction

Industry 4.0 has been quickly advancing in the past few years, viewed as next-generation revolutionary technology for industrial manufacturing and production, which is featured by introduction and implementation of advanced technologies, such as artificial intelligence [1,2], cyber-physical systems, the internet of things, and cloud computing [3–6]. Large-scale machine-to-machine (M2M) communication and internet of things are integrated for increased automation, improved communication, self-monitoring, and production of smart machines [7], which could analyze and diagnose issues without the need for human involvement, enabling more efficient processes, safer working environments, and better quality and productivity.

In the context of Industry 4.0, oilfield industries call for efficient and cost-effective oil production. In the operation and management of the oilfield, a new concept called the “smart oilfield” is introduced [8], which is based on big data, the internet of things, and other technologies to automatically measure, analyze, and optimize oil production [9,10]. Recently, some companies with a strategic vision, such as Shell’s NaKika Field [11], Xinjiang Oilfield [12], and Schlumberger’s Haradh Smart Oilfield [13], have already started construction of smart oilfields.

Smart oilfields rely on a high-surveillance environment, via real-time data transmission, interactive business collaboration, and efficient decision-making processes [14–16]. Therefore, the large-scale information exchange among different parts is indispensable, which highly depends on the network layer (soft technologies [1–6]) and the physical layer (optical fiber links). On one hand, some wireless techniques are used in some oilfields for data communication. Because the oil will is dispersedly distributed, using remote wireless monitoring is convenient [17]; however, the communication quality is susceptible to atmospheric turbulence. In contrast, fiber communication could obtain high stability. In recent years, space-division multiplexing, including mode-division multiplexing using multimode fibers or few-mode fibers and core multiplexing using multicore fibers, has been proposed and could expand the transmission capacity to overcome the single-mode fiber capacity limit. On the other hand, for fiber sensing in smart oilfields, various parameters could be monitored based on Rayleigh scattering, Raman scattering, and Brillouin scattering. To date, the data transmission and parameter monitoring are two separate parts, and it is difficult to build integrated systems, leading to the high cost of transmitters, receivers, and the process of deploying fibers. Therefore, there is an urgent need for special fiber links for both increased data transmission capacity and distributed sensing with high sensitivity [18]. Naturally, multicore optical fibers can be expected to play a critical role in smart oilfields in which parts of cores are responsible for data transmission, while other cores are used for sensing.

Multicore fibers, a significant component of space-division multiplexing, have been investigated for a few decades and are thought to be a strong candidate to meet the exponential growth of capacity demand [19,20]. On the other hand, in the area of optical sensing, there have been some reports about utilizing multicore fibers to measure multi variables, such as vibration, temperature, and strain [18,21–23]. For smart oilfields, compared with normal single-mode fibers, a unique characteristic of multicore fiber is that bending would generate local tangential strain in off-center cores, and the strain is angular-position-dependent. The cores in off-center positions lead to high bending sensitivity [24]. However, although multicore fiber design has been developed for a long time, it is still challenging to propose an integrated multicore fiber for smart oilfields applications due to the design complexity, which should take into account the performance of each core itself and the crosstalk between the adjacent cores. For digital transmission cores, the main goal is to realize low differential mode group delay (DMGD) because the computational complexity of digital signal processing (DSP) increases with that, and low DSP complexity is the basis of real-time transmission, which is limited by the processing capability of the widely used chips. As for analog transmission cores, the effective area (A_{eff}) should be enlarged to depress the nonlinear effect due to the watt-scale input power [25]. To maintain the accuracy and the sensitivity of sensing, the arrangement of different types of cores should be considered and the core pitches between neighboring cores should be optimized to keep the stability of the signal transmission. However, to date, there are few reports about multicore fiber design especially for smart oilfields, which could support real-time data transmission, device-to-device networking, and variables monitoring at the same time.

In this paper, we propose a heterogeneously integrated seven-core fiber for interconnection and awareness applications in smart oilfields, which could not only support digital and analog signal transmission but could also measure temperature and vibration through Raman effect and phase-sensitive optical time-domain reflectometry. The core arranged in the center is used for digital transmission to maintain communication stability, while others are arranged around the center for analog transmission and sensing, with equal pitches to increase sensing sensitivity. The core for digital signal transmission has a low differential mode group delay of 10 ps/km over the C-band and the crosstalk between adjacent cores is lower than −55 dB/km at the pitch of 50 μm. A 25-Gbaud transmission over 50 km is simulated. Each core for analog signal transmission has a large effective area of 172 μm^2 to suppress the nonlinear effect due to the watt-scale input power. In all, the proposed heterogeneously integrated multicore fiber exhibits great potential to be applied in smart oilfields, meeting the demand for efficient and cost-effective oil production.

2. A Case Study

To make the design process more targeted, the proposed heterogeneously integrated multicore fiber in this paper is based on the demand of a company named Beijing Perception Technology Company [26]. Figure 1 shows the schematic of the smart oilfields composed of oil production area, data distribution area, and office area.

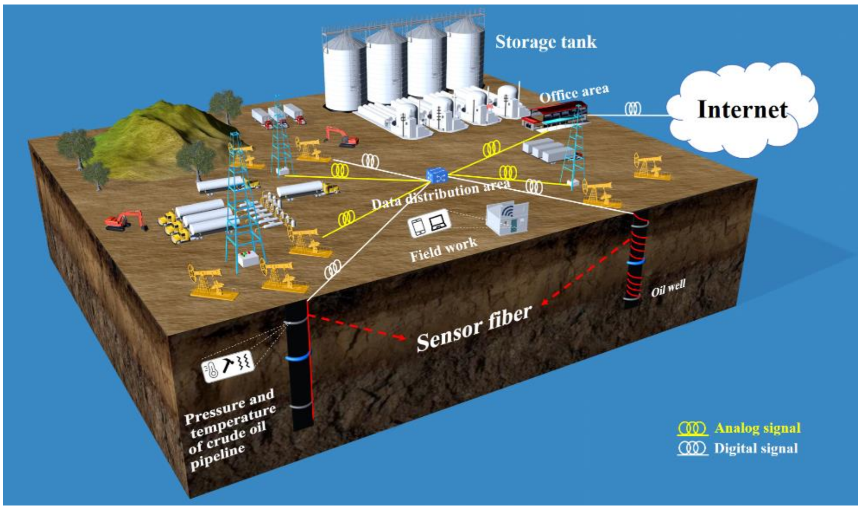

Figure 1. Schematic of the smart oilfields, which are consisted of production area, data distribution area, and office area.

The company is in urgent need of multifunctional fiber to support the construction of smart oilfields. In the production area, simultaneous distributed intrusion detection and temperature monitoring of pipelines are needed in order to achieve real-time alarm on excavation, theft, leakage, and other potential threats. This could be accomplished by implementing a Raman optical time-domain reflectometry (ROTDR) and phase-sensitive optical time-domain reflectometry (φ-OTDR) hybrid sensing system, where the ROTDR is used to monitor the temperature change and φ-OTDR is used for real-time vibration detection [18]. As for data interaction, the data throughput of the oilfield is approximately 1 Tbits per day, and it might keep increasing at a high speed in the near future. Therefore, we propose a three-mode six-polarization core for digital transmission and set the highest baud rate as 25 G with a quadrature phase-shift keying (QPSK) modulation format, which could obtain 0.3 Tbit/s and enough would be available for the situation, even for an instantaneous sharp increase of data. To realize the real-time transmission, a big challenge is the DSP complexity due to the limitation of the processing capacity of field programmable gate arrays (FPGAs). Although some companies, such as XILINX and Altera [27,28], have made a breakthrough in high-performance FPGAs, these products are not cost-effective and cannot be widely used at present. We set the filter taps as 32, which means a common FPGA could meet the demand. Moreover, the oilfields are mostly located in remote areas with weak signals. In this sense, it is essential to transmit analog signals to build a temporary network for connecting the devices and correspondence. Compared with long-haul transmission, fibers in smart oilfields might be used for short-distance transmission, so the maximum transmission distance is set as 50 km.

3. Heterogeneously Integrated Multicore Fibers

The proposed heterogeneously integrated multicore fiber could simultaneously support digital signal transmission, analog signal transmission, and temperature and vibration measurement. The schematic of the designed fiber is shown in Figure 2. It can be seen that different cores are responsible for different functions. To maintain the stability of digital signals and depress the bending loss, cores for digital transmission are set in the center of the cladding, while cores for sensing and analog transmission are arranged alternately in the outside circle. The numbers and types of different cores are determined by the demand of data rates and application scenarios. In addition, the pitch between adjacent cores is another key parameter needing to be optimized due to the trade-off between crosstalk and bending loss with a limited diameter of cladding. The cladding diameter should not be larger than 200 μm to guarantee mechanical reliability [29]. To maintain a crosstalk lower than −50 dB/km, the core pitch is set as 50 μm. To reduce micro bending loss, the outer cladding thickness is set as 40 μm. Therefore, the cladding diameter is 180 μm.

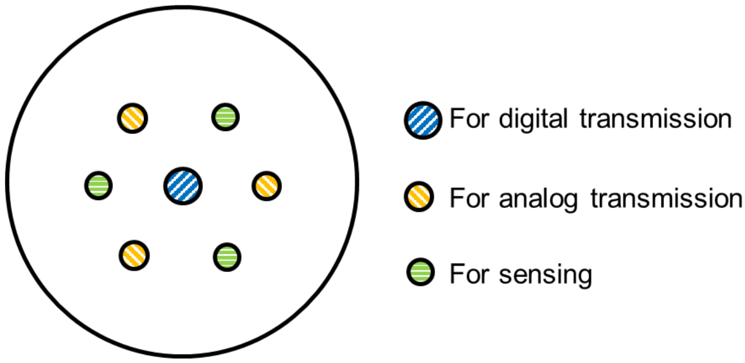

Figure 2. Schematic of the designed heterogeneous 7-core multicore fiber.

In general, there are three types of fibers: step-index (SI) fibers, grade-index (GI) fibers, and trench-assisted (TA) fibers. From the perspective of the manufacturing process, SI fibers and GI fibers are easier to fabricate than TA fibers due to their relatively simple structures. However, TA fibers could be designed by optimizing the width and depth of the trench and other parameters to obtain high performance, such as low DMGD or large A_{eff}. Figure 3 reveals the refractive index profiles of various types of fibers. r_{core}, w_1, and w_2 are the core radius, the distance between the core and the trench, and the width of the trench, respectively. α is the gradient parameter determined by the shape of the refractive index profile.

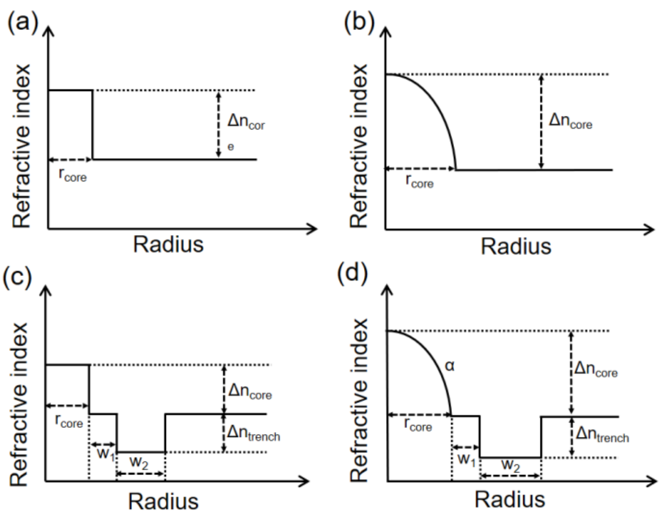

Figure 3. Refractive index profiles of various types of fibers. (**a**) step-index fiber, (**b**) graded-index fiber, (**c**) step-index trench-assisted fiber, (**d**) graded-index trench-assisted fiber.

3.1. Design of Digital Transmission Cores

For fiber design, the choice of structure is dependent on the applications. The key consideration for digital signal transmission is DMGD because the computational complexity of DSP increases with it, and the level of DSP complexity determines whether the real-time transmission could be realized. We sweep the parameters, including r_{core}, α, and

Δn_{core}, and the setting of ranges follows two principles. One is the ranges should be as large as possible and the other is the designed fiber should only support three guide modes. We calculate the DMGD over the C-band based on full vector finite element analysis. The group delay of any propagation mode in FMF is given by [30]

$$\tau_g = \frac{z(n_{eff} - \lambda \frac{dn_{eff}}{d\lambda})}{c} \quad (1)$$

where z represents transmission distance, c is the speed of light in vacuum, λ is the wavelength and n_{eff} is the effective refraction index. Therefore, the DMGD between LP_{mn} mode and LP_{01} mode is given by:

$$\text{DMGD} = \frac{\left(n_{eff}^{LP_{mn}} - \lambda \frac{dn_{eff}^{LP_{mn}}}{d\lambda}\right)}{c} - \frac{\left(n_{eff}^{LP_{01}} - \lambda \frac{dn_{eff}^{LP_{01}}}{d\lambda}\right)}{c} \quad (2)$$

The DMGD results are shown in Figure 4.

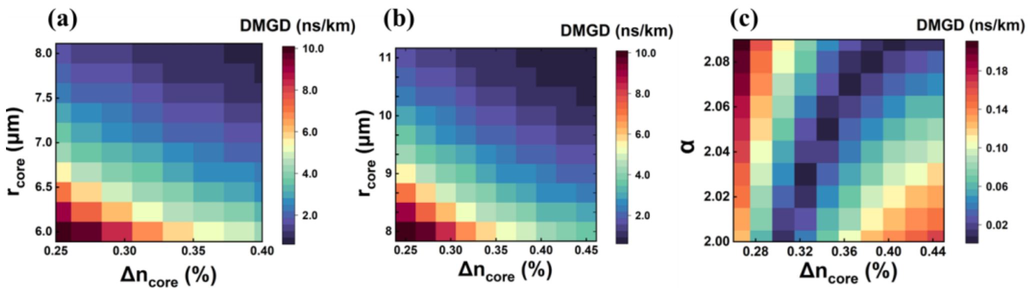

Figure 4. The DMGD variation of digital transmission cores with the setting parameters. (**a**) sweeping r_{core} and Δn_{core}, (**b**) sweeping r_{core} and Δn_{core}, and the α is 2, (**c**) sweeping α and Δn_{core}, and the r_{core} is 10.5 μm.

Within the sweeping ranges, the DMGD of GI fibers and TA-GI fibers have inflection points, while that of SI fibers have a gradual decrease with the increment of r_{core}, and Δn_{core}. We list the parameters of the three types of fibers at their lowest DMGD levels in Table 1, and the lowest DMGD of the TA-GI fiber is only 10 ps/km, which is 1/18 of the DMGD of SI fiber (183 ps/km) and one percent of that of the GI fiber (1000 ps/km). Although low DMGD could be obtained in the TA-GI fiber, the manufacturing process is more complex than that of SI fibers. In a word, it is not possible to use the GI fiber as the digital transmission core in this scene, and the choice of the SI fiber or the TA-GI fiber is dependent on the DSP complexity tolerance, which is positively correlated with DMGD. In addition, bending loss is considered and calculated by the finite element method. The bending radius is defined as the radius when the loss of the highest guided mode is 0.5 dB/turn, and the bending radius is calculated by the method in [31]. For the SI fiber, GI fiber, and TA-GI fiber, the bending radii are 70 mm, 30 mm and 20 mm. A smaller bending radius means better anti-bending performance. Considering the applied conditions in smart oilfields, the bending radius is m-scale or even larger, the anti-bending performance of the designed fiber is up to standard. A phrase.

Table 1. The parameters of various types of fibers applied for digital transmission.

Type	r_{core} (μm)	Δn_{core} (%)	Δn_{trench} (%)	α	w_1 (μm)	w_2 (μm)
SI	7.1	0.27	\	\	\	\
GI	10.5	0.40	\	2	\	\
TA-GI	10.5	0.345	0.34	2.05	2	9.3

3.2. Design of Analog Transmission Cores

As for the design of the analog transmission cores, A_{eff} should be enlarged to depress the nonlinear effect. For analog signal transmission, the input power is watt-scale (~10 dBm), which is 10 times larger than that of digital transmission (~0 dBm) [32]. The A_{eff} of standard G.654E fiber is approximately 120 μm^2. To obtain a larger A_{eff}, we only excite the fundamental mode in a three-mode fiber. In smart oilfields, the transmission distance is usually less than 50 km, and there are few intra-link splices. The multipath interference (MPI) in this scenario is approximately −40 dB, which sightly limits transmission performance [33]. As for the connection of transmitters and receivers, the MPI could be induced by the mismatch between mode fields. Low-loss mode field adapters produced by stepwise reverse tapering technique and thermally expanded core technique could further effectively reduce the MPI [34]. Referring to the design of cores for digital transmission, the results are shown in Figure 5 and Table 2. It shows that the A_{eff} variation of the TA-SI fiber is smaller than that of the other two types within the sweeping ranges, which means that TA-SI fibers could maintain the stability of large A_{eff} in a larger range. When the A_{eff} is set as 172 μm^2, the bending radii of the SI-fiber, GI-fiber and TA-SI fiber are 50 mm, 80 mm, and 40 mm, respectively.

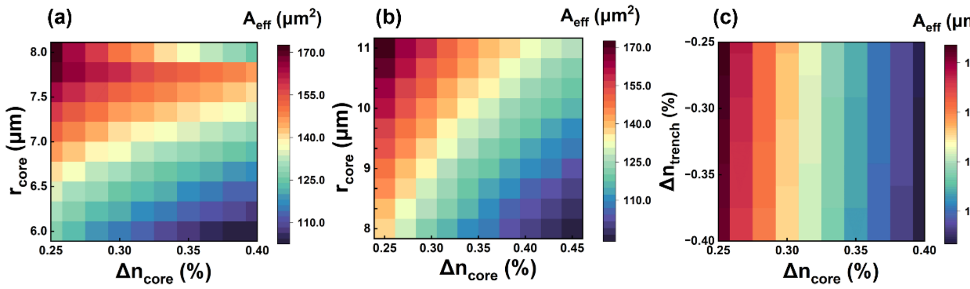

Figure 5. The A_{eff} variation of analog transmission cores with the setting parameters. (**a**) sweeping r_{core} and Δn_{core}, (**b**) sweeping r_{core} and Δn_{core}, and α is 2, (**c**) sweeping Δn_{trench} and Δn_{core}, and r_{core} is 8 μm.

Table 2. The parameters of various types of fibers applied for analog transmission.

Type	r_{core} (μm)	Δn_{core} (%)	Δn_{trench} (%)	α	w_1 (μm)	w_2 (μm)
SI	8.0	0.27	\	\	\	\
GI	11.0	0.25	\	2	\	\
TA-SI	8.0	0.25	0.25	\	4	5

3.3. The Analysis of the Crosstalk

To maintain the signal quality, the crosstalk between adjacent cores, which is calculated by the finite element method to evaluate the performance of the multicore fiber, should be lower than −55 dB/km [35]. As we mentioned above, the cores for digital transmission and analog transmission support three modes while the core for analog transmission only excites the fundamental mode. For sensing cores, we use the standard G.652 fiber. We know that the distance between the edges of cores influences crosstalk greatly and it is a negative correlation with the crosstalk. To simplify the calculation, we suppose that the crosstalk between two three-mode cores is the crosstalk of the whole multicore fiber because the core radius of G.652 fiber (3 μm) is much smaller than the other two three-mode fibers, which leads to lower crosstalk when the core pitch is fixed. The parameters of cores for digital transmission and analog transmission are listed in Tables 1 and 2. The bending radius is assumed as one meter according to the diameter of the pipeline. The crosstalk

(XT) is obtained by using coupled-power theory [36]. The mode-coupling coefficient could be shown as:

$$\kappa_{pq} = \frac{\omega\varepsilon_0 \iint_{-\infty}^{+\infty} \left(N^2 - N_q^2\right) E_p^* \cdot E_q dxdy}{\iint_{-\infty}^{+\infty} u_z \cdot \left(E_p^* \times H_p + E_p \times H_p^*\right) dxdy} \tag{3}$$

where ω is an angular frequency of the sinusoidally varying electromagnetic fields, ε_0 is the permittivity of the medium, and u_z means the outward-directed unit vector. E_p and E_q represent the electric field distribution of core inside the range of core p, and the electric field distribution of core inside the range of core q, respectively. The crosstalk (XT) between the neighboring cores with length L is estimated as:

$$XT = \tanh\left(\overline{h}_{pq}\mathrm{L}\right) \tag{4}$$

$$h_{pq}(z) = \frac{2\mathrm{K}_{pq}^2 d}{1 + \left(\Delta\beta'_{pq} d\right)^2} \tag{5}$$

where K_{pq} is the average value of κ_{pq} and κ_{qp}. $\Delta\beta'_{pq}$ is the difference of equivalent propagation constant between two cores. d means the correlation length [37]. Here, d is assumed to be 0.05 m.

Figure 6 shows the crosstalk as a function of the pitch between neighboring cores. It could be seen that the crosstalk reduces as the core pitch increases. To compare all the combinations, we set the core pitch as 50 µm. For each row, the third combination performs better than the other two, which means that we could obtain a better performance if the SI-TA fiber is applied in the analog-transmission core. For example, in the first row, the core for digital transmission is the SI fiber and that for analog transmission is the SI fiber, the GI fiber, and the SI-TA fiber, respectively. The maximum crosstalk of the third combination is −63.4 dB/km, while the other two combinations' maximum crosstalk values are approximately −55.4 dB/km and −34.1 dB/km. Furthermore, comparing the results by column is another dimension. In the third column, when the SI-TA structure is used for analog transmission, there is a slight difference among the three combinations, but the maximum crosstalk values of them are all lower than −55 dB/km, which satisfies the communication requirements of crosstalk. Above all, we suppose that the core for analog transmission should use the SI-TA fiber and that for digital transmission could be chosen from the SI fiber or the GI-TA fiber, depending on the processing capability of chips.

3.4. Transmission System Demonstration

To further investigate the performance of the multicore fiber in actual applicable conditions, we model the signal transmission process in VPItransmissionMaker Optical Systems. A 100 Gb/s quadrature phase-shift keying (QPSK) signal is generated at 1550 nm, and the input powers of the digital signal and the analog signal are 0 dBm and 13 dBm, respectively. The core pitch is set as 50 µm. The number of splices is 2 and the splice loss is 0.4 dB. The loss of LP_{01} and LP_{11} is 0.20 dB/km and 0.22 dB/km, respectively. The mode crosstalk is −60 dB/km. In the simulation, the fan-in and fan-out devices and (de)multiplexers are somewhat ideal devices. The crosstalk of these two types of devices is −50 dB, and the insertion loss is 1 dB and 3 dB, respectively. Taking into account the processing capacity of widely used chips, the number of taps is set as 32 to maintain the possibility of real-time transmission. The DSP algorithm is referred to in [38], which could adjust the distribution of filter taps and enhance the utilization to efficiently recover signal. The SI-TA fiber is set as the core for analog transmission. The Q^2-factor performances versus different transmission distances with the digital signal transmission cores of the SI fiber, the GI-TA fiber, and the fabricated GI-TA fiber are shown in Figure 7. Because the designed fiber would be applied in smart oilfields, the maximum transmission distance is set as 50 km. The Q^2-factor threshold of forward error correction (FEC) is 6.5 dB, which is recommended by IEEE Standard 802.3 [39]. We could see that when the core for digital transmission is the optimized low-DMGD three-mode TA-GI fiber, the Q^2-factors of two guided modes decrease slightly as the length increases and those are over 15 dB within 50 km. Compared with this, if the SI fiber is set as the core for digital transmission, the Q^2-factor of each guided mode decreases more sharply from approximately 15 dB to 6 dB. The effective transmission distance is approximately 43 km, which is smaller than 50 km. It shows that the performance of the TA-GI fiber is more available and could be applied in this environment. As for analog transmission performance, due to the 13 dBm input power of analog signal transmission, it is almost 20 times larger than the input power of digital signal transmission. For such an asymmetry channel, the performance of the analog single transmission is almost the same as that in a single-core transmission system.

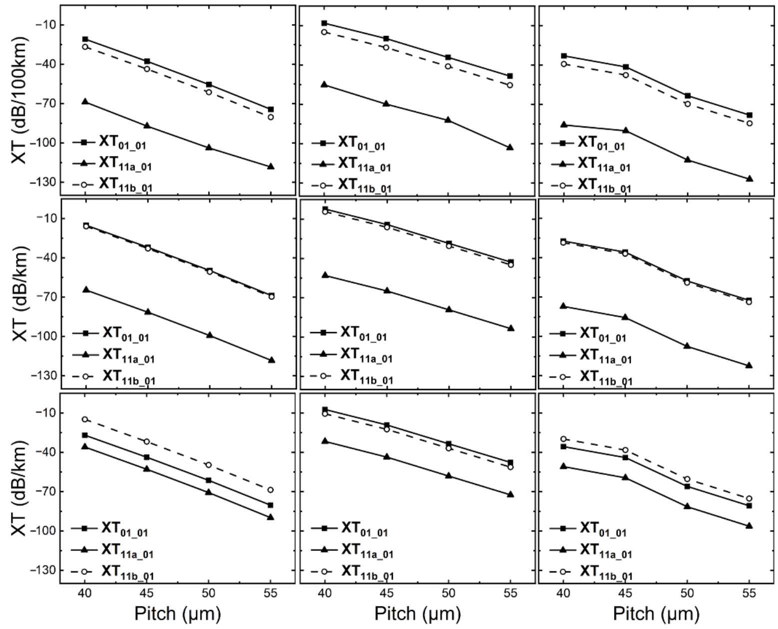

Figure 6. The relationship between the crosstalk of guided modes and the core pitches. In each row, the cores for digital transmission are the SI fiber, the GI fiber, and the GI-TA fiber. In each column, the cores for analog transmission are the SI fiber, the GI fiber, and the SI-TA fiber, respectively.

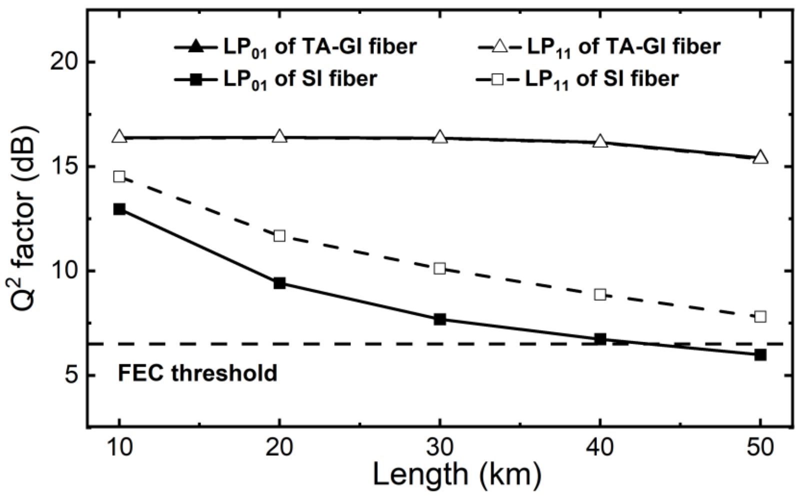

Figure 7. Q^2 factor performances versus transmission distances with different types of fibers for digital transmission.

4. Conclusions

In this paper, we propose a heterogeneously integrated seven-core fiber for smart oilfields, which could not only support digital and analog signal transmission but could also measure temperature and vibration through Raman effect and phase-sensitive optical time-domain reflectometry. The core arranged in the center is used for digital transmission to maintain communication stability, while others are arranged around the center for analog transmission and sensing, with equal pitches to increase sensing sensitivity. The core for digital signal transmission has a low differential mode group delay of 10 ps/km over the C-band. Each core for analog signal transmission has a large effective area of 172 μm^2 to suppress the nonlinear effect. The crosstalk between adjacent cores is lower than -55 dB/km, which could support 25-Gbaud real-time transmission over 50 km, based on widely used chips for data processing. We believe that the proposed multicore fiber could support and enhance the construction of smart oilfields.

Author Contributions: X.W. planned and wrote the paper. H.S. contributed to the plotting of Figure 3. H.W. contributed to the writing of the fourth part. Y.L. took the overall responsibility for managing the manuscript. Z.Y. and Z.H. revised the whole article and gave advice. L.Z. supervised the work and provided technical leadership. All co-authors contributed to the final version with suggestions and critical comments. All authors have read and agreed to the published version of the manuscript.

Funding: This research was funded by the National Key R&D Program of China under grant 2019YFB2203902, the National Natural Science Foundation of China under grant 62105241, and the Postgraduate Research Program of Tianjin under grant 2021YJSB129.

Institutional Review Board Statement: Not applicable.

Informed Consent Statement: Not applicable.

Data Availability Statement: Not applicable.

Acknowledgments: The authors would like to thank the anonymous reviewers for their valuable comments and suggestions to improve this manuscript.

Conflicts of Interest: The authors declare no conflict of interest.

References

1. Nilsson, N.J. *Principles of Artificial Intelligence*; Morgan Kaufmann: San Mateo, CA, USA, 1982.
2. Jordan, M.I.; Mitchell, T.M. Machine learning: Trends, perspectives, and prospects. *Science* **2015**, *349*, 255–260. [CrossRef] [PubMed]
3. Lee, E.A. Cyber physical systems: Design challenges. In Proceedings of the IEEE Symposium on Object/Component/Service-Oriented Real-Time Distributed Computing, Orlando, FL, USA, 5–7 May 2008; pp. 363–369.
4. Armbrust, M.; Fox, A.; Griffith, R.; Joseph, A.D.; Katz, R.; Konwinski, A.; Lee, G.; Patterson, D.; Rabkin, A.; Stoica, I.; et al. A view of cloud computing. *Commun. ACM* **2010**, *53*, 50–58. [CrossRef]
5. Atzori, L.; Iera, A.; Morabito, G. The Internet of Things: A survey. *Comput. Netw.* **2010**, *54*, 2787–2805. [CrossRef]
6. Wang, S.; Wan, J.; Li, D.; Zhang, C. Implementing smart factory of industrie 4.0: An outlook. *Int. J. Distrib. Sens. Netw.* **2016**, *12*, 3159805. [CrossRef]
7. Weyrich, M.; Schmidt, J.-P.; Ebert, C. Machine-to-machine communication. *IEEE Softw.* **2014**, *31*, 19–23. [CrossRef]
8. Du, D.; Zhang, X.; Guo, Q.; Zhang, B.; Zhang, G. Smart oilfield technology. In Proceedings of the International Field Exploration and Development Conference, Xi'an, China, 18–20 September 2018; pp. 685–694.
9. Ahmad, I.; Pothuganti, K. Smart field monitoring using ToxTrac: A cyber-physical system approach in agriculture. In Proceedings of the International Conference on Smart Electronics and Communication, Trichy, India, 10–12 September 2020; pp. 723–727.
10. Eifert, T.; Eisen, K.; Maiwald, M.; Herwig, C. Current and future requirements to industrial analytical infrastructure—Part 2: Smart sensors. *Anal. Bioanal. Chem.* **2020**, *412*, 2037–2045. [CrossRef]
11. Available online: https://www.shell.com (accessed on 21 November 2022).
12. Available online: https://www.quantum.com/zh-cn/resources/customer-success/xinjiang-oilfield-company/ (accessed on 21 November 2022).
13. Available online: https://www.slb.com (accessed on 21 November 2022).
14. Temizel, C.; Canbaz, C.H.; Palabiyik, Y.; Putra, D.; Asena, A.; Ranjith, R.; Jongkittinarukorn, K. A comprehensive review of smart/intelligent oilfield technologies and applications in the oil and gas industry. In Proceedings of the SPE Middle East Oil and Gas Show and Conference, Manama, Bahrain, 18–21 March 2019.

15. Al-Subaiei, D.; Al-Hamer, M.; Al-Zaidan, A.; Nawaz, M.S. Smart production surveillance: Production monitoring and optimization using integrated digital oil field. In Proceedings of the SPE Kuwait Oil and Gas Show and Conference, Mishref, Kuwait, 13–16 October 2019.
16. Carvajal, G.; Maucec, M.; Cullick, S. Components of artificial intelligence and data analytics. In *Intelligent Digital Oil and Gas Fields*, 1st ed.; Gulf Professional Publishing: Boston, MA, USA, 2018; pp. 101–148.
17. Hussain, R.F.; Salehi, M.A.; Kovalenko, A.; Feng, Y.; Semiari, O. Federated Edge Computing for Disaster Management in Remote Smart Oil Fields. In Proceedings of the 2019 IEEE 21st International Conference on High Performance Computing and Communications; IEEE 17th International Conference on Smart City; IEEE 5th International Conference on Data Science and Systems (HPCC/SmartCity/DSS), Zhangjiajie, China, 10–12 August 2019; pp. 929–936.
18. Lu, P.; Lalam, N.; Badar, M.; Liu, B.; Chorpening, B.T.; Buric, M.P.; Ohodnicki, P.R. Distributed optical fiber sensing: Review and perspective. *Appl. Phys. Rev.* **2019**, *6*, 041302. [CrossRef]
19. Li, G.; Bai, N.; Zhao, N.; Xia, C. Space-division multiplexing: The next frontier in optical communication. *Adv. Opt. Photon.* **2014**, *6*, 413–487. [CrossRef]
20. Saitoh, K.; Matsuo, S. Multicore Fiber Technology. *J. Light. Technol.* **2016**, *34*, 55–66. [CrossRef]
21. Dang, Y.; Zhao, Z.; Wang, X.; Liao, R.; Lu, C. Simultaneous distributed vibration and temperature sensing using multicore fiber. *IEEE Access* **2019**, *7*, 151818–151826. [CrossRef]
22. Zhao, Z.; Dang, Y.; Tang, M.; Li, B.; Gan, L.; Fu, S.; Wei, H.; Tong, W.; Shum, P.; Liu, D. Spatial-division multiplexed Brillouin distributed sensing based on a heterogeneous multicore fiber. *Opt. Lett.* **2017**, *42*, 171–174. [CrossRef] [PubMed]
23. Yan, B.; Li, J.; Zhang, M.; Xu, Y.; Yu, T.; Zhang, J.; Qiao, L.; Wang, T. Temperature accuracy and resolution improvement for a Raman distributed fiber-optics sensor by using the Rayleigh noise suppression method. *Appl. Opt.* **2020**, *59*, 22–27. [CrossRef] [PubMed]
24. Zhao, Z.Y.; Tang, M.; Lu, C. Distributed multicore fiber sensors. *Opto-Electron. Adv* **2020**, *3*, 190024. [CrossRef]
25. Zhang, L.; Agarwal, A.M.; Kimerling, L.C.; Michel, J. Nonlinear Group IV photonics based on silicon and germanium: From near-infrared to mid-infrared. *Nanophotonics* **2014**, *3*, 247–268. [CrossRef]
26. Available online: http://www.zjofs.com (accessed on 21 November 2022).
27. Available online: https://www.xilinx.com (accessed on 21 November 2022).
28. Available online: https://www.intel.com/content/www/us/en/products/programmable.html (accessed on 21 November 2022).
29. Matsui, T.; Nakajima, K.; Fukai, C. Applicability of Photonic Crystal Fiber with Uniform Air-Hole Structure to High-Speed and Wide-Band Transmission Over Conventional Telecommunication Bands. *J. Light. Technol.* **2009**, *27*, 5410–5416. [CrossRef]
30. Zhang, H.; Zhao, J.; Yang, Z.Q.; Peng, G.J.; Di, Z.X. Low-DMGD, Large-Effective-Area and Low-Bending-Loss 12-LP-Mode Fiber for Mode-Division-Multiplexing. *IEEE Photonics J.* **2019**, *11*, 1–8. [CrossRef]
31. Tu, J.; Saitoh, K.; Koshiba, M.; Takenaga, K.; Matsuo, S. Design and analysis of large-effective-area heterogeneous trench-assisted multi-core fiber. *Opt. Express* **2012**, *20*, 15157–15170. [CrossRef]
32. Wen, H.; Zheng, H.; Mo, Q.; Velázquez-Benítez, A.M.; Xia, C.; Huang, B.; Liu, H.; Yu, H.; Sillard, P.; Lopez, J.E.A.; et al. Few-mode fibre-optic microwave photonic links. *Light Sci. Appl.* **2017**, *6*, e17021. [CrossRef]
33. Downie, J.D.; Mlejnek, M.; Roudas, I.; Wood, W.A.; Zakharian, A.; Hurley, J.E.; Mishra, S.; Yaman, F.; Zhang, S.; Ip, E.; et al. Quasi-Single-Mode Fiber Transmission for Optical Communications. *IEEE J. Sel. Top. Quantum Electron.* **2017**, *23*, 31–42. [CrossRef]
34. Yang, L.; Yang, Z.; Xu, T.; Hou, L.; Zhou, R.; Gan, L.; Cao, S.; Xiao, X.; Zhang, L. Low-loss Mode Field Adapter Using Reverse Tapering for Fundamental Mode Transmission over MMFs. In Proceedings of the Optical Fiber Communication Conference (OFC) 2022, San Diego, CA, USA, 6 March 2022; p. M4E.7.
35. Xie, Y.; Pei, L.; Zheng, J.; Zhao, Q.; Ning, T.; Li, J. Low-DMD and low-crosstalk few-mode multi-core fiber with air-trench/holes assisted graded-index profile. *Opt. Commun.* **2020**, *474*, 126155. [CrossRef]
36. Marcuse, D. Derivation of Coupled Power Equations. *Bell Syst. Tech. J.* **1972**, *51*, 229–237. [CrossRef]
37. Tu, J.; Saitoh, K.; Koshiba, M.; Takenaga, K.; Matsuo, S. Optimized Design Method for Bend-Insensitive Heterogeneous Trench-Assisted Multi-Core Fiber with Ultra-Low Crosstalk and High Core Density. *J. Light. Technol.* **2013**, *31*, 2590–2598. [CrossRef]
38. Arık, S.Ö.; Askarov, D.; Kahn, J.M. Adaptive Frequency-Domain Equalization in Mode-Division Multiplexing Systems. *J. Light. Technol.* **2014**, *32*, 1841–1852. [CrossRef]
39. IEEE. *IEEE Std 802.3bt-2018 (Amendment to IEEE Std 802.3-2018 as amended by IEEE Std 802.3cb-2018)*; IEEE Standard for Ethernet Amendment 2: Physical Layer and Management Parameters for Power over Ethernet over 4 Pairs. IEEE: Piscataway Township, NJ, USA, 2019; pp. 1–291. [CrossRef]